THE JOURNAL OF BIOLOGICAL CHEMISTRY VOL. 290, NO. 41, pp. 25090–25102, October 9, 2015

Phosphorylation-induced Conformational Ensemble Switching in an Intrinsically Disordered Cancer/Testis Antigen*

Received for publication, April 13, 2015, and in revised form, July 29, 2015 Published, JBC Papers in Press, August 4, 2015, DOI 10.1074/jbc.M115.658583

Yanan He[‡§], Yihong Chen[‡§], Steven M. Mooney[¶], Krithika Rajagopalan[¶1], Ajay Bhargava[‖], Elizabeth Sacho[**], Keith Weninger[**], Philip N. Bryan[‡], Prakash Kulkarni[¶2], and John Orban[‡§3]

From the [‡]W. M. Keck Laboratory for Structural Biology, University of Maryland Institute for Bioscience and Biotechnology Research, Rockville, Maryland 20850, the [§]Department of Chemistry and Biochemistry, University of Maryland, College Park, Maryland 20742, the [¶]Department of Urology, Johns Hopkins University School of Medicine, Baltimore, Maryland 21287, [‖]Shakti BioResearch, Woodbridge, Connecticut 06525, and the [**]Department of Physics, North Carolina State University, Raleigh, North Carolina 27695

Background: PAGE4, an intrinsically disordered protein up-regulated in prostate cancer, binds to c-Jun and potentiates its transactivation.
Results: The effects of phosphorylation on PAGE4 conformation, dynamics, and c-Jun binding were determined by NMR.
Conclusion: Phosphorylation induces a more compact conformational ensemble, restricting access to the c-Jun binding site.
Significance: This study may help to explain how phosphorylation of PAGE4 alters its binding to c-Jun.

Prostate-associated gene 4 (PAGE4) is an intrinsically disordered cancer/testis antigen that is up-regulated in the fetal and diseased human prostate. Knocking down PAGE4 expression results in cell death, whereas its overexpression leads to a growth advantage of prostate cancer cells (Zeng, Y., He, Y., Yang, F., Mooney, S. M., Getzenberg, R. H., Orban, J., and Kulkarni, P. (2011) The cancer/testis antigen prostate-associated gene 4 (PAGE4) is a highly intrinsically disordered protein. *J. Biol. Chem.* 286, 13985–13994). Phosphorylation of PAGE4 at Thr-51 is critical for potentiating c-Jun transactivation, an important factor in controlling cell growth, apoptosis, and stress response. Using NMR spectroscopy, we show that the PAGE4 polypeptide chain has local and long-range conformational preferences that are perturbed by site-specific phosphorylation at Thr-51. The population of transient turn-like structures increases upon phosphorylation in an ~20-residue acidic region centered on Thr-51. This central region therefore becomes more compact and more negatively charged, with increasing intramolecular contacts to basic sequence motifs near the N and C termini. Although flexibility is decreased in the central region of phospho-PAGE4, the polypeptide chain remains highly dynamic overall. PAGE4 utilizes a transient helical structure adjacent to the central acidic region to bind c-Jun with low affinity *in vitro*. The binding interaction is attenuated by phosphorylation at Thr-51, most likely because of masking the effects of the more compact phosphorylated state. Therefore, phosphorylation of PAGE4 leads to conformational shifts in the dynamic ensemble, with large functional consequences. The changes in the structural ensemble induced by posttranslational modifications are similar conceptually to the conformational switching events seen in some marginally stable ("metamorphic") folded proteins in response to mutation or environmental triggers.

Prostate-associated gene 4 (PAGE4) is a 102-amino acid member of the PAGE[4] family of cancer/testis antigens, a heterogeneous group of proteins typically expressed in testicular germ cells. They remain silent in most somatic tissues but are aberrantly expressed in several types of cancer (1, 2). More than 200 cancer/testis antigens have been reported to date (3), and these are broadly divided into two groups: the CT-X antigens, located on the X chromosome, and the non-X CT antigens, located on various autosomes. Although the non-X CT antigens are evolutionarily well conserved, the CT-X antigens, with the possible exception of the MAGE family, appear to lack orthologues in lower vertebrates beyond primates (4, 5), suggesting that these proteins have evolved relatively recently. Because of the lack of phylogenetic conservation, the functions of most, if not all, CT-X antigens remain poorly understood both in gametogenesis and tumorigenesis (2, 6, 7). Moreover,

* This study was supported, in whole or in part, by National Institutes of Health Grants CA181730 (to J. O. and P. K.) and GM62154 (to J. O. and P. B.). The NMR facility is jointly supported by the University of Maryland, the National Institute of Standards and Technology, and a grant from the W. M. Keck Foundation. The authors declare that they have no conflicts of interest with the contents of this article.
The NMR assignments for WT PAGE4 and phospho-PAGE4 have been deposited in the Biological Magnetic Resonance Bank under accession numbers 26544 and 26545, respectively.
[1] Present address: Dept. of Biological Sciences, Columbia University, NY, NY 10027.
[2] Present address: University of Maryland Institute for Bioscience and Biotechnology Research, Rockville, MD 20850. To whom correspondence may be addressed: Tel.: 240-314-6122; E-mail: pkulkar4@ibbr.umd.edu.
[3] To whom correspondence may be addressed: University of Maryland Institute for Bioscience and Biotechnology Research, Rockville, MD 20850. Tel.: 240-314-6221; E-mail: jorban@umd.edu.

[4] The abbreviations used are: PAGE, prostate-associated gene; CT, cancer/testis; IDP, intrinsically disordered protein; PRE, paramagnetic relaxation enhancement; MTSL, (1-oxyl-2,2,5,5- tetramethylpyrroline-3-methyl) methane-thio-sulfonate; I_{ox}, paramagnetic state; I_{red}, diamagnetic state; MAGE, melanoma-associated antigen; HSQC, heteronuclear single quantum coherence; PSI-BLAST, position-specific iterative basic local alignment search tool.

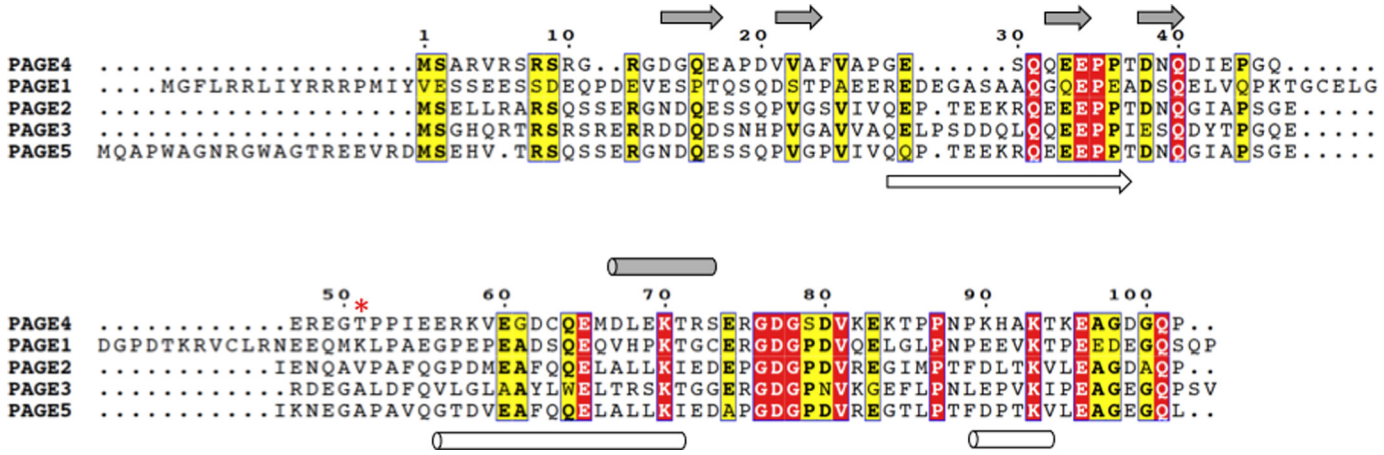

FIGURE 1. **Amino acid sequence alignment of the PAGE family of human proteins.** Similar and invariant residues are highlighted in *yellow* and *red columns*, respectively. Alignment was carried out using ESPript. Local conformational preferences of PAGE4 determined in this study are shown in *gray* at the top of the alignment. Transient β-extended and helical structures are represented by *arrows* and *cylinders*, respectively. PAGE5 preferences from an earlier study (29) are shown in *white* at the bottom of the alignment.

an overwhelming majority (>95%) of CT-X antigens are predicted to be intrinsically disordered proteins (IDPs) (8). IDPs are proteins or regions within structured proteins that lack a rigid three-dimensional structure but play important roles in many biological processes, such as transcriptional regulation, cell division, and signaling (9–11).

The PAGE family belongs to the CT-X group of antigens and consists of multiple members (PAGE1–5) that share significant sequence homology (Fig. 1). Although all PAGE genes are expressed in the testes of the adult human, PAGE4 is the only member of this family that is expressed in the normal prostate, in this case during development (12). In fact, PAGE4 is remarkably prostate-specific (12, 13), with dynamic expression patterns in the human male, suggesting that the protein may function as a proto-oncogene. The PAGE4 protein is highly expressed in the developing fetal prostate (12, 14) but is barely detectable in the normal adult gland (12). However, the PAGE4 protein is up-regulated in both symptomatic benign prostatic hyperplasia, which is related to prostate cancer (13), and in prostate cancer itself (12, 15, 16), indicating a potential role for PAGE4 in disease pathology. Consistent with this hypothesis, knocking down PAGE4 expression results in cell death, whereas its overexpression leads to a growth advantage of prostate cancer cells (17).

Protein isolates of PAGE4 from the prostate cancer cell line PC3 are phosphorylated predominantly at Thr-51 by homeodomain-interacting protein kinase 1 (HIPK1) (18). Furthermore, a cell-based luciferase assay demonstrates that PAGE4 dramatically potentiates transactivation by c-Jun (14) and that phosphorylation at Thr-51 is critical for this process (18). c-Jun is an essential component of the AP-1 complex, a family of early response transcription factors with important roles in the control of cell growth, apoptosis, and stress response (19). Together, these and other results (12) indicate that PAGE4 is a stress-response protein and a component of the HIPK1-JNK1-c-Jun-activated stress response pathway (18). The amplifying effect on c-Jun transactivation suggests that PAGE4 may modulate the activity of AP-1. Notably, c-Jun is also up-regulated in the developing (20) and diseased prostate (21–26), whereas the AP-1 complex is up-regulated in symptomatic benign prostatic hyperplasia (27) as well as in prostate cancer (28). These patterns are coincident with PAGE4 expression (13) and underscore the importance of the PAGE4/c-Jun interactions in prostatic development and disease.

Previous biophysical characterization using single-molecule FRET experiments have indicated that the non-phosphorylated WT PAGE4 protein interacts with c-Jun (14) and that phosphorylation at Thr-51 by HIPK1 attenuates this interaction (18), suggesting a conformational switching mechanism upon phosphorylation. Here we describe, at a single-residue level, how phosphorylation perturbs the local and global structural features of PAGE4 and provide a possible explanation for the change in binding to c-Jun. To our knowledge, this is the first detailed study on the effects of phosphorylation in an intrinsically disordered CT-X antigen family member that plays an important role in the diseased prostate. Only one other completely disordered CT-X antigen has been investigated from a biophysical perspective to date, a splice variant of PAGE5 that lacks part of the N terminus (29). However, the biological function(s) of PAGE5 in the prostate and the effect of posttranslational modifications on its structure and function remain unknown. This study indicates that phosphorylation on Thr-51 induces conformational and dynamic switching in the PAGE4 ensemble, leading to a new cellular function. This is similar conceptually to the expanded function observed for both naturally occurring and designed proteins that can switch their fold topologies (30, 31).

Experimental Procedures

Sample Preparation—The PAGE4 gene was cloned into an eXact tag pPAL8 vector system. This construct places two purification tags, His_6 and the subtilisin prodomain, at the N terminus, and these tags are subsequently removed on an engineered subtilisin column (32). ^{15}N- and $^{13}C/^{15}N$-labeled samples were prepared using ^{15}N-labeled ammonium chloride and uniformly labeled ^{13}C-labeled glucose as the sole nitrogen and carbon sources. The His_6-prodomain-PAGE4 construct was transformed into BL21DE3 *Escherichia coli* cells and grown in M9

minimal media at 37 °C until the A_{600} reached 0.6–0.9. Protein expression was induced with 1 mM isopropyl 1-thio-β-D-galactopyranoside at 25 °C for 18 h. Cells were harvested by centrifugation at 1200 × *g* for 30 min, resuspended in buffer A (6 M guanidinium hydrochloride, 20 mM NaPi, and 500 mM NaCl (pH 7.8)), and lysed by sonication. After pelleting (1 h, 10,000 × *g*), the soluble extract was purified on a nickel-nitrilotriacetic acid column with the following steps: successive column washes with buffer B (8 M urea, 20 mM NaPi, and 500 mM NaCl (pH 7.8)), buffer C (8 M urea, 20 mM NaPi, and 500 mM NaCl (pH 6.0)), buffer C plus 10 mM imidazole, and buffer C plus 20 mM imidazole; equilibration of the column with buffer D (100 mM KPi (pH 7.0)); and elution with buffer D plus 350 mM imidazole. Fractions containing purified His_6-prodomain-PAGE4 protein were collected and loaded onto a subtilisin S189 column for cleavage of the His_6 prodomain as follows: step 1, wash with buffer D (2 column volumes); step 2, wash with 2 M sodium acetate solution (1 column volume) and then buffer D (2 column volumes); step 3, repeat step 2 two times; step 4, wash with buffer D (2 column volumes); step 5, elute with 10 mM sodium azide in buffer D. PAGE4-containing fractions more than 95% pure by gel analysis were combined and concentrated for further study. Protein concentration was measured using a colorimetric assay (33). Mutant constructs of PAGE4 were prepared employing the Q5 site-directed mutagenesis kit (New England Biolabs) and were expressed and purified as above.

Phosphorylated PAGE4 was prepared by coexpression with a pET28a gene construct for the kinase domain of human HIPK1. Both the PAGE4 and HIPK1 constructs were cotransformed into BL21DE3 *E. coli* cells and grown in M9 minimal media with ^{15}N- or $^{13}C/^{15}N$ labels to an A_{600} of ~0.6–0.9 at 37 °C. Protein expression was induced with 1 mM isopropyl 1-thio-β-D-galactopyranoside for 18 h at 25 °C. Phosphorylated PAGE4 was then purified using the procedure described above.

NMR Spectroscopy—Sample concentrations of 200 μM WT PAGE4 and ~150 μM phospho-PAGE4 were used in 100 mM KPi, 10 mM NaN_3, and 0.1 mM DTT. NMR spectra were recorded at 10 °C on a Bruker Avance III 600-MHz spectrometer equipped with a Z-gradient $^1H/^{13}C/^{15}N$ cryoprobe. Backbone resonances were assigned using the following three-dimensional triple resonance experiments: HNCACB, CBCA (CO)NH, HNCO, HN(CA)CO, and (H)N(CA)NNH. Side chain assignments were made using three-dimensional C(CO)NH-TOCSY and H(CCO)NH-TOCSY experiments. Three-dimensional ^{15}N-edited NOESY and three-dimensional ^{13}C-edited NOESY spectra were acquired on both PAGE4 and phospho-PAGE4 using a mixing time of 150 ms. Multidimensional NMR spectra were processed with NMRPipe (34) and analyzed using SPARKY (35).

A comparison of PAGE4 C^α chemical shifts with random coil values (36) was made, where $\Delta C^\alpha = C^\alpha{}_{exp} - C^\alpha{}_{rc}$. The $^3J_{HNH\alpha}$ coupling constants were obtained from a three-dimensional HNHA experiment (37). $\Delta^3J_{HNH\alpha}$ values were determined by taking the difference between experimental coupling constants and residue-dependent values obtained from model peptide studies (38). Heteronuclear $\{^1H\}$-^{15}N steady-state NOEs were measured using standard procedures (39). A relaxation delay of 5 s was used between experiments. Dynamics experiments were carried out in quadruplicate, and values are reported as mean ± S.D. Amide exchange rates were measured using the CLEANEX-PM pulse program (40) with mixing times of 5, 10, 15, 20, and 25 ms.

Paramagnetic relaxation enhancement (PRE) experiments were carried out initially using 50 μM ^{15}N-labeled WT-PAGE4 or ^{15}N-labeled phospho-PAGE4, spin-labeled with (1-oxyl-2,2,5,5- tetramethylpyrroline-3-methyl)methane-thio-sulfonate (MTSL, Santa Cruz Biotechnology) at the single naturally occurring cysteine, Cys-63. Additional PRE experiments were performed using non-phosphorylated and HIPK1-phosphorylated versions of the mutants [^{15}N]-S7C-C63A-PAGE4 and [^{15}N]-N88C-C63A-PAGE4. PAGE4 samples were reacted at room temperature with 10 molar equivalents of MTSL from a 1 M stock solution in acetonitrile, and the reaction was followed to completion (~1–2 h) by MALDI-mass spectrometry. Spin-labeled PAGE4 samples were dialyzed to remove excess MTSL. ^{15}N HSQC spectra (256 ^{15}N increments) were acquired on MTSL-labeled samples and on samples treated with DTT (5 equivalents). Peak intensities for the paramagnetic (I_{ox}) and diamagnetic (I_{red}) states were measured using SPARKY. As a control for intermolecular effects, a 50 μM sample of [^{14}N]-WT-PAGE4-C63-MTSL was mixed with a 50 μM sample of [^{15}N]-WT-PAGE4-C63A. Spectra and peak intensities were obtained for the I_{ox} and I_{red} states as above.

Structural model calculations were carried out using CNS 1.3 (41) with standard simulated annealing and torsion angle dynamics protocols, including code for radius of gyration restraints (42). Calculations were initiated from a random coil polypeptide chain. Radius of gyration restraints from single-molecule FRET data (14) were employed for WT-PAGE4 (radius of gyration, ~33.3 Å) and Thr(P)-51 PAGE4 (radius of gyration, ~28.6 Å). Distance restraints were obtained from NOE and PRE data. Interproton NOE restraints were on the basis of peak intensities and categorized as weak (2.8–4.0 Å) or very weak (2.8–6.0 Å). PRE distance restraints were obtained from I_{ox}/I_{red} values. For residues with $I_{ox}/I_{red} \leq 0.8$, a bounds restraint of 20–25 Å was used between the C^α atom of the cysteine residue with the MTSL spin label and the amide groups of the relevant residues. For residues with $I_{ox}/I_{red} \leq 0.6$, a bounds restraint of 15–25 Å was utilized. For residues with I_{ox}/I_{red} ~1, a lower bound restraint of 25 Å was employed between the corresponding amide groups and the C^α atom of the cysteine residue with the spin label. An ensemble of 1000 structures was calculated for WT-PAGE4 and Thr(P)-51 PAGE4, and the 20 lowest energy conformers with no violations greater than 1 Å were displayed for each using PyMOL (43).

PAGE4/c-Jun Experiments—Full-length human c-Jun (331 residues) and truncated c-Jun-223 (residues 1–223) and c-Jun (residues 150–331) were prepared and purified using methods described previously (18). Shorter c-Jun fragments, c-Jun-60 (residues 1–60), c-Jun-90 (residues 1–90), and c-Jun-150 (residues 1–150), were constructed using standard cloning procedures with cleavable N-terminal His tags, overexpressed in BL21DE3 *E. coli* cells, and purified with nickel-nitrilotriacetic acid columns. NMR titrations of either 10 μM ^{15}N-labeled WT-PAGE4 or phospho-PAGE4 with unlabeled c-Jun were carried out in 100 mM KPi, 10 mM NaN_3, and 0.1

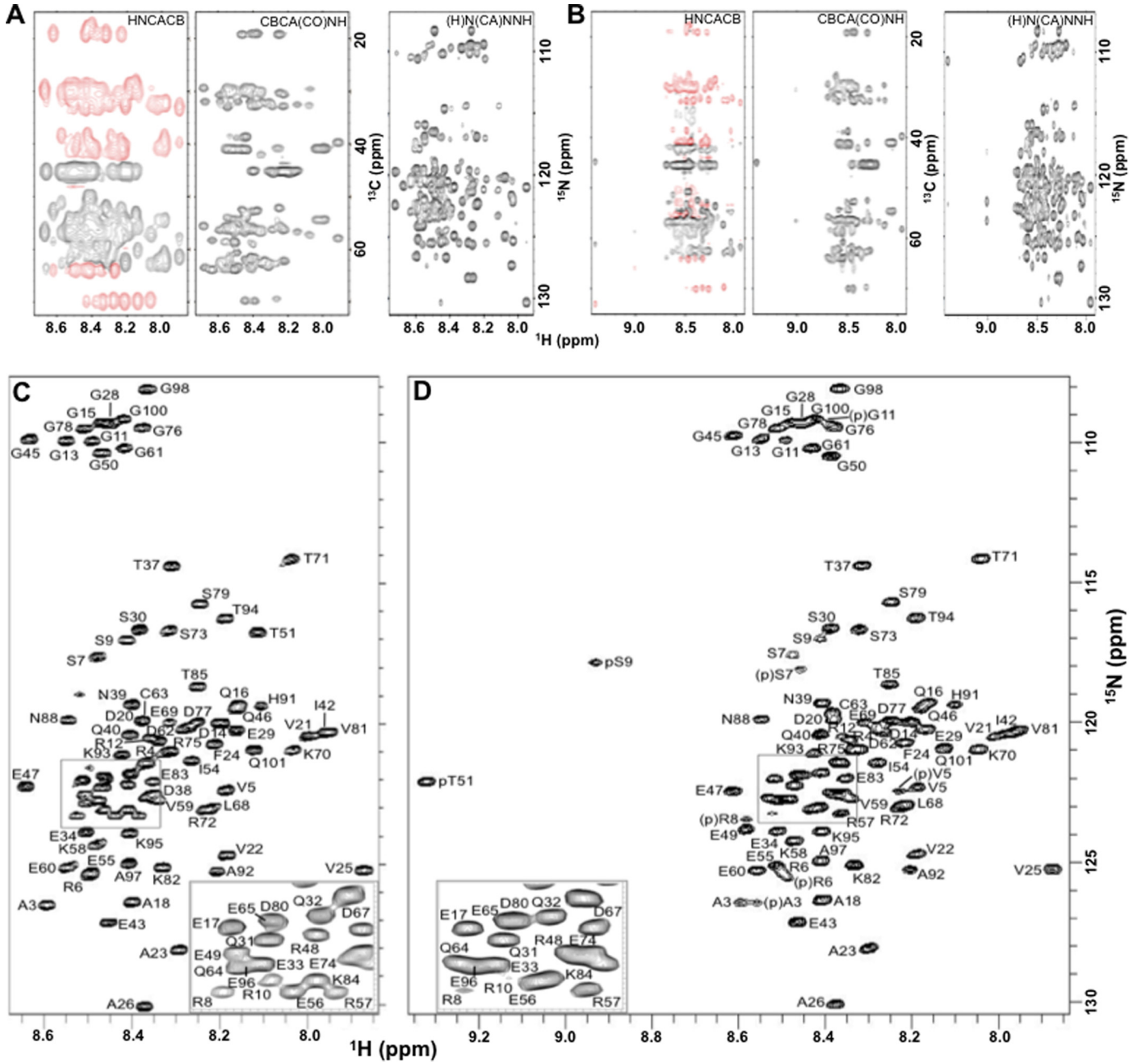

FIGURE 2. **PAGE4 NMR data and assignments.** *A*, two-dimensional compressed planes from three-dimensional HNCACB (*left panel*), CBCA(CO)NH (*center panel*), and (H)N(CA)NNH (*right panel*) spectra for WT (non-phosphorylated) PAGE4. *B*, the same spectra for HIPK1-phosphorylated PAGE4. *C*, two-dimensional ^{1}H-^{15}N HSQC spectrum of WT-PAGE4 with main chain assignments. *Inset*, expanded view of the *boxed region*. *D*, two-dimensional ^{1}H-^{15}N HSQC spectrum of phosphorylated PAGE4. The phosphorylated residues are indicated as *pS9* and *pT51*. Because phosphorylation at Ser-9 is partial, residues of both non-phosphorylated and phosphorylated states were assigned. Assignments for residues neighboring the phosphorylated Ser(P)-9 are indicated (*e.g. (p)S7*).

mM DTT. Two-dimensional ^{15}N HSQC spectra were acquired as a function of increasing c-Jun concentration. c-Jun fragments 1–60, 1–90, and 1–150 were added to identical buffer up to 6 molar equivalents. c-Jun (1–223) or full-length c-Jun were added up to 3 molar equivalents. A reverse titration was also performed using 30 μM ^{15}N-labeled c-Jun (residues 150–331) with up to 4 molar equivalents of unlabeled WT-PAGE4. Chemical shift perturbations were determined using standard methods from $\Delta\delta_{total} = [(W_H\Delta\delta_H)^2 + (W_N\Delta\delta_N)^2]^{1/2}$, where $W_H = 1$ and $W_N = 0.2$. The cell-based luciferase assays were carried out in triplicate utilizing prostate cancer PC3 cells, as described previously (18).

Results

Sample Preparation and NMR Assignments—WT-PAGE4 samples were prepared using the eXact tag purification system, which has the advantage over most other methods of providing the desired naturally occurring polypeptide chain with no additional residues at either end (32). This is particularly useful for the study of IDPs, where the high flexibility of the chain allows

for the possibility that extraneous terminal residues could influence the analysis of conformation and dynamics through non-native transient interactions.

Two-dimensional ^{1}H-^{15}N HSQC spectra were recorded over a range of temperatures from 5–35 °C. The spectra recorded at 10 °C gave the best resolution and the most backbone amide peaks, and therefore assignments were carried out at this temperature. The traditional mode of backbone assignment utilizing HNCACB and CBCA(CO)NH experiments led to some ambiguity in C^{α}/C^{β} connectivities, arising from highly similar chemical shift patterns. This was resolved partially by establishing connectivity through carbonyl shifts with HNCO and HN(CA)CO experiments. Amide-to-amide connectivities, obtained from the (H)N(CA)NNH experiment (44, 45), were particularly useful in resolving the remaining uncertainties and validating the final set of assignments. As an additional validation step, a number of residues were mutated (S7A, S9A, S30A, and C63A) in separate samples to confirm their assignment. Using this approach, all of the main chain amides in the WT PAGE4 NMR spectrum were assigned to their corresponding residues in the sequence (Fig. 2, *A* and *C*). Side chain assignments were made from the backbone amide identities using H(CCO)NH-TOCSY and C(CO)NH-TOCSY experiments.

Phosphorylation of WT PAGE4 was achieved by coexpression with the kinase domain of HIPK1, previously identified to act on PAGE4 through an extensive screen of ~200 kinases (18). The original HIPK1 kinase study suggested single-site specificity of phosphorylation at Thr-51, but the coexpression experiments carried out here on a larger scale for NMR analysis produced an ~2:1 mixture of singly and doubly phosphorylated PAGE4, evident from both NMR analysis (Fig. 2, *B* and *D*) and mass spectrometry (Fig. 3). NMR assignment of phospho-PAGE4 using the above methods revealed complete phosphorylation at Thr-51 and partial (~30–40%) phosphorylation at Ser-9. Main chain amides in both singly and doubly phosphorylated PAGE4 were completely assigned (Fig. 2*D*). In particular, the residues around the secondary phosphorylation site at Ser-9 could be distinguished from the corresponding residues where Ser-9 is not phosphorylated. Although phosphorylation at Thr-51 plays a key role in the function of PAGE4, the functional relevance of Ser-9 phosphorylation has yet to be investigated.

Local Conformational Preferences—With near-complete backbone NMR assignments in hand for both WT PAGE4 and Thr(P)-51 PAGE4, the effects of phosphorylation at Thr-51 on backbone chemical shifts (^{15}N, H^{N}, C^{α}, and CO) were measured (Fig. 4). As expected, the largest effects for ^{15}N, H^{N}, and CO shifts were seen at Thr-51 itself, with relatively smaller changes for the nearest neighbors. In contrast to these localized effects, significant differences were detected for C^{α} chemical shifts over a region extending from residues 40–70 (Fig. 4*C*). Because C^{α} shifts are a sensitive indicator of structure (46, 47), this suggested that phosphorylation at Thr-51 induces sequential, medium-range, and even longer-range changes in conformational preferences.

Further analysis of experimental C^{α} and C^{β} chemical shifts was carried out by comparison with sequence-corrected random coil values calculated from model peptides (36, 48). These

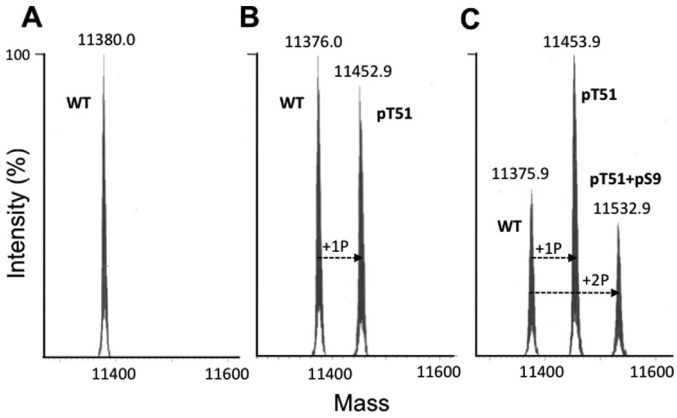

FIGURE 3. **Monitoring phosphorylation of PAGE4 by mass spectrometry.** *A* and *B*, mass spectra of WT PAGE4 as a control (A) and after incubation with HIPK1 and ATP at 30 °C for 3 h (*B*) and 12 h (*C*).

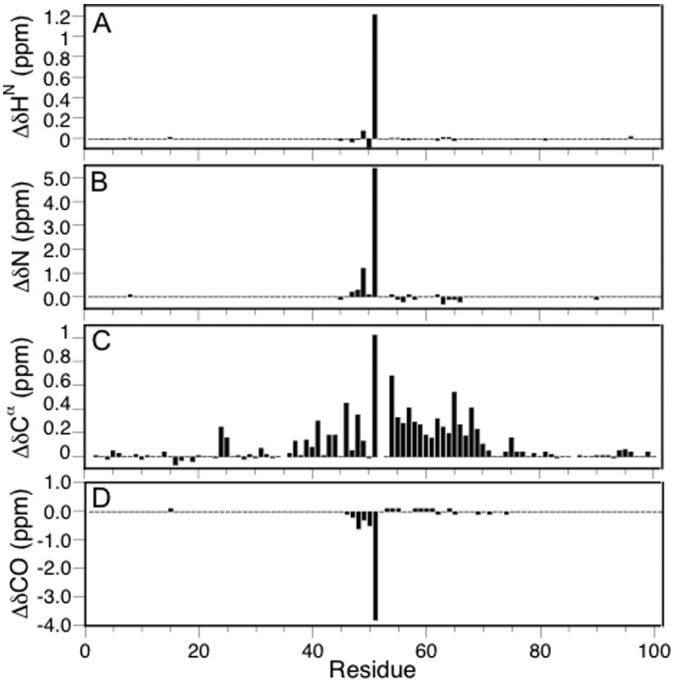

FIGURE 4. **Main chain chemical shift changes in PAGE4 upon phosphorylation where $\Delta\delta = \delta$(Thr(P)-51 PAGE4) $- \delta$(WT).** *A*, $\Delta\delta H^{N}$. *B*, $\Delta\delta N$. *C*, $\Delta\delta C^{\alpha}$. *D*, $\Delta\delta CO$. Estimated errors in chemical shift differences were on the basis of spectra recorded for two different PAGE4 samples and were as follows: ^{1}H, 0.01 ppm; ^{15}N, 0.025 ppm; ^{13}C, 0.1 ppm.

data indicate that the WT PAGE4 polypeptide chain has considerable intrinsic disorder but also has contiguous residues with propensities for β-extended conformations ($\Delta C^{\alpha}<0$, $\Delta C^{\beta}>0$; residues 14–17, 21–23, 32–34, and 38–40) and α-helical conformations ($\Delta C^{\alpha}>0$, $\Delta C^{\beta}<0$; residues 67–73) (Fig. 5, *A* and *B*). On the basis of comparison with ΔC^{α} values for fully folded proteins, these regions are ~10–20% transiently ordered. Phosphorylation does not significantly alter local conformational preferences in the N-terminal half of the molecule but gives more positive ΔC^{α} values around Thr-51 that extend into the transient helical region.

Additional lines of evidence from $^{3}J_{HNH\alpha}$ coupling constants that report on the backbone Φ torsion angle (Fig. 5*C*) and interproton NOEs (Fig. 5*D*) are generally consistent with the conformational preferences obtained from chemical shifts. Contig-

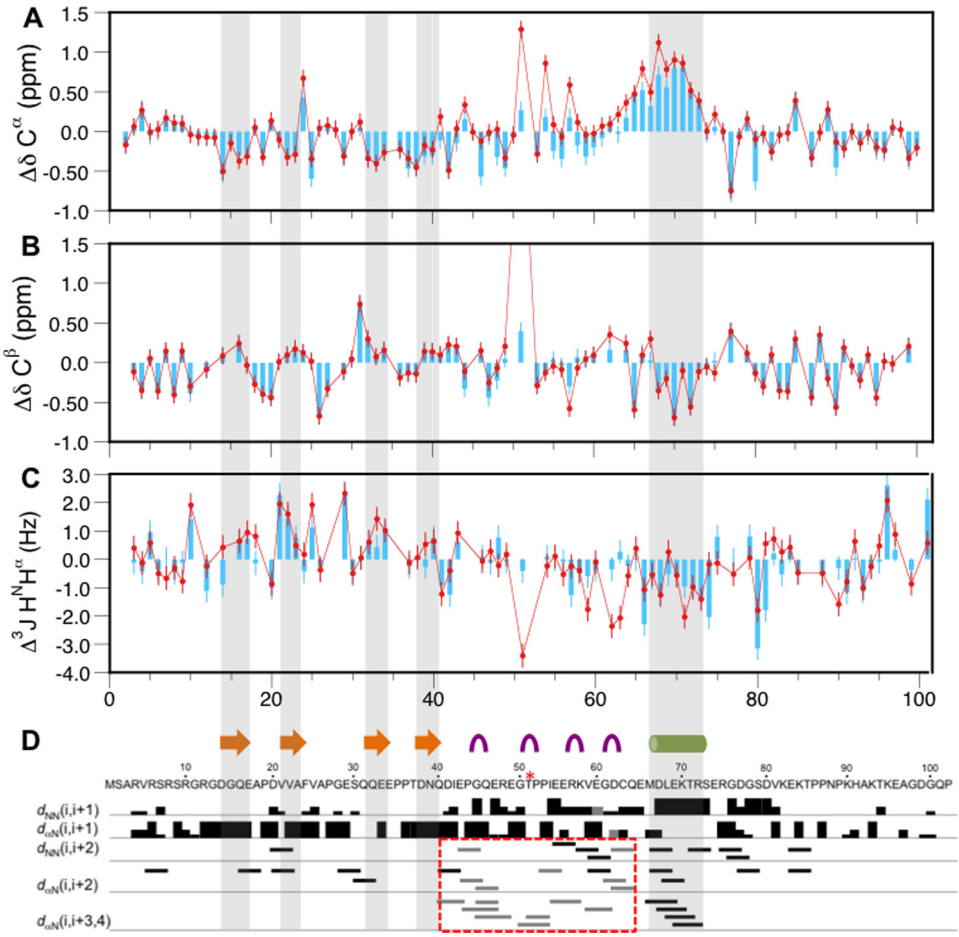

FIGURE 5. **Summary of local conformational preferences for PAGE4.** *A*, C^{α} secondary chemical shift differences for WT PAGE4 (*blue*) and pT51-PAGE4 (*red*). Stretches of residues with positive values indicate α-helical tendencies, whereas negative regions indicate extended β-type structures. *B*, C^{β} chemical shift differences between experimental and random coil values for WT PAGE4 (*blue*) and Thr(P)-51 PAGE4 (*red*). Consecutive residues with negative values indicate helical preferences, whereas positive values occur in extended regions. The estimated error in *A* and *B* is on the basis of ^{13}C chemical shift changes in two different WT PAGE4 samples. *C*, differences between experimental and random coil values of the $^{3}J_{HNH\alpha}$ coupling constants for WT PAGE4 (*blue*) and Thr(P)-51 PAGE4 (*red*). Negative regions indicate α-helical propensity, and positive regions reflect extended β structures. The coupling constant error is estimated to be ~0.4 Hz on the basis of the signal-to-noise ratio in HNHA experiments. *D*, sequential and medium-range backbone interproton NOEs observed for WT PAGE4 and Thr(P)-51 PAGE4. NOEs detected in Thr(P)-51 PAGE4 but not WT PAGE4 are shown as *gray bars* (*red box*). The intensity of NOEs is indicated by the height of the bars. The secondary structural preferences are summarized above the amino acid sequence as follows: *orange*, β-type structure; *green*, α-helix; *purple*, turn-like structures.

uous negative $\Delta^{3}J_{HNH\alpha}$ values ($= J_{exp}$-J_{rc}) (38) correspond with turn-like and helical structures, whereas contiguous positive values correspond with β-extended conformations. Regions of relatively strong sequential $d_{\alpha N}(i, i+1)$ NOEs match with extended conformations in the N-terminal half of PAGE4, whereas the longest stretch of $d_{NN}(i, i+1)$ NOEs overlaps with the transient helical region. Notably, numerous $(i, i+2)$ and $(i, i+3)$ NOEs are present in the region between residues 41–63 in phospho-PAGE4 but not WT PAGE4 (Fig. 5*D*). Together, the chemical shift, coupling constant, and NOE data point toward an increased population of turn-like structures around Thr-51 upon phosphorylation. The turn structures in PAGE4 have flexible conformations that are not tightly defined because of the limited number of experimental restraints.

The proline residues adjacent to the primary phosphorylation site, Pro-52 and Pro-53, have been shown to be primarily (>90%) *trans* isomers on the basis of either C^{γ} chemical shift analysis (49) or the characteristic $d_{\alpha\delta}(i, i+1)$ NOE pattern in a three-dimensional ^{13}C-edited NOESY spectrum. Indeed, using this analysis, all prolines in PAGE4 are mainly *trans* in both WT-PAGE4 and phospho-PAGE4. Evidence for a significantly populated intraresidue hydrogen bond between Thr-51H^{N} and one of the oxygen atoms of the Thr-51 phosphoryl group comes from the large downfield perturbation in ^{1}H chemical shift (~1.3 ppm) (Fig. 2*D*) as well as the slowed amide proton exchange rate of Thr-51 upon phosphorylation (Fig. 6*A*). On the basis of the degree of protection from exchange ($p = k_{ex}^{WT}/k_{ex}^{phospho}$), this hydrogen bond provides ~2 kcal/mol of stabilization (50, 51). Phosphorylation of Thr-51 also protects neighboring residues (Arg-48, Gly-50, and Glu-55) from exchange, but to a lesser extent (Fig. 6*B*), reflecting the lower solvent accessibility of amides in this region.

Global Conformational Preferences—In addition to local conformational preferences, longer-range interactions within the structural ensemble can be probed using PRE methods (52). This involves introduction of a stable paramagnetic species, in this case a nitroxide spin label, at a defined point in the polypeptide chain through covalent cysteine-mediated attachment

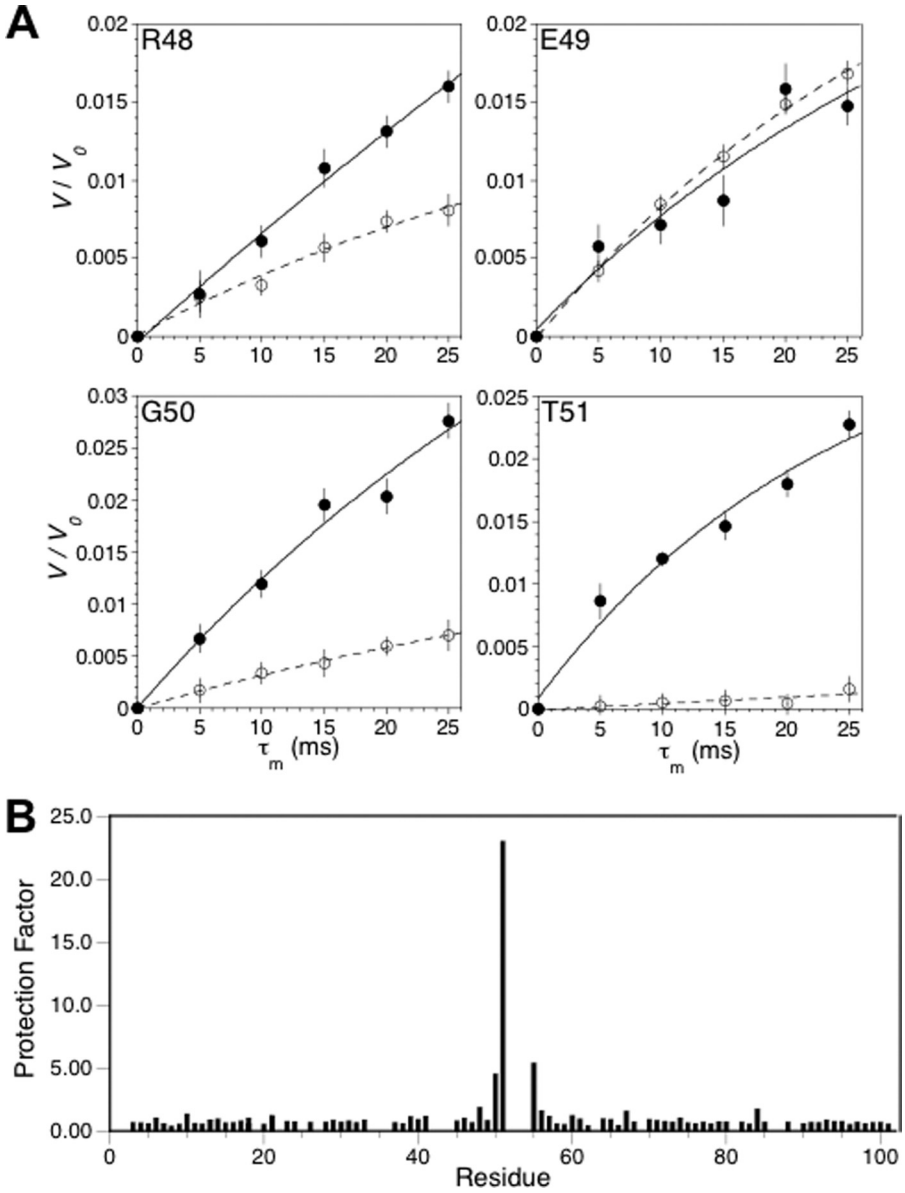

FIGURE 6. **Amide hydrogen exchange in PAGE4.** *A*, representative plots for WT PAGE4 (*filled circles*) and Thr(P)-51 PAGE4 (*open circles*). *V* is the peak volume from a CLEANEX-PM experiment at mixing times of 5–25 ms. V_o is the reference peak volume measured from a fast HSQC spectrum. Errors in V/V_o are estimated on the basis of the signal-to-noise ratio. *B*, protection factor (k_{WT}/k_P) as a function of residue number. The experimental error in protection factors is estimated to be ± 50%.

of MTSL, followed by measurement of amide peak intensities in the presence (I_{ox}) and absence (I_{red}) of the spin label. The native PAGE4 amino acid sequence has a unique cysteine, Cys-63, that is centrally located and well positioned to assess PRE effects for both the non-phosphorylated and phosphorylated protein.

The results show that the WT PAGE4 conformational ensemble exhibits preferred long-range contacts and that phosphorylation modulates these interactions. On average, residues that are within 25 Å of Cys-63 display a PRE effect ($I_{ox}/I_{red} < 1$). These include the amino acids that neighbor Cys-63, with the nearest neighbors having the largest effects, and continue out from the position of the spin label to ~12 residues in both directions. Furthermore, there are significant PRE effects outside of this nearest neighbor envelope, with long-range contacts to residues 3–13 and 82–93 (Fig. 7*A*). Phosphorylation alters these long-range preferences, increasing the PRE effects (smaller I_{ox}/I_{red} values) in both the N- and C-terminal regions. A control experiment with a 1:1 mixture of [^{14}N]-WT-PAGE4-C63-MTSL and [^{15}N]-C63A-PAGE4 showed no measurable interactions between the spin label on one chain and ^{15}N-labeled amide protons on the other, indicating that the PRE effects observed are intramolecular (Fig. 7*A*). Spin labels were also placed near the N terminus and C terminus using S7C-C63A and N88C-C63A PAGE4 mutants, respectively. Experiments on these samples demonstrated reciprocal PRE effects on the central region of the polypeptide chain, which were enhanced upon phosphorylation (Fig. 7, *B* and *C*).

On the basis of these results, conservative PRE and NOE restraints were used as inputs for calculating ensemble conformations for both WT PAGE4 and phosphorylated PAGE4. Although not all restraints are likely to be satisfied simultaneously in a single polypeptide chain, the resulting models pro-

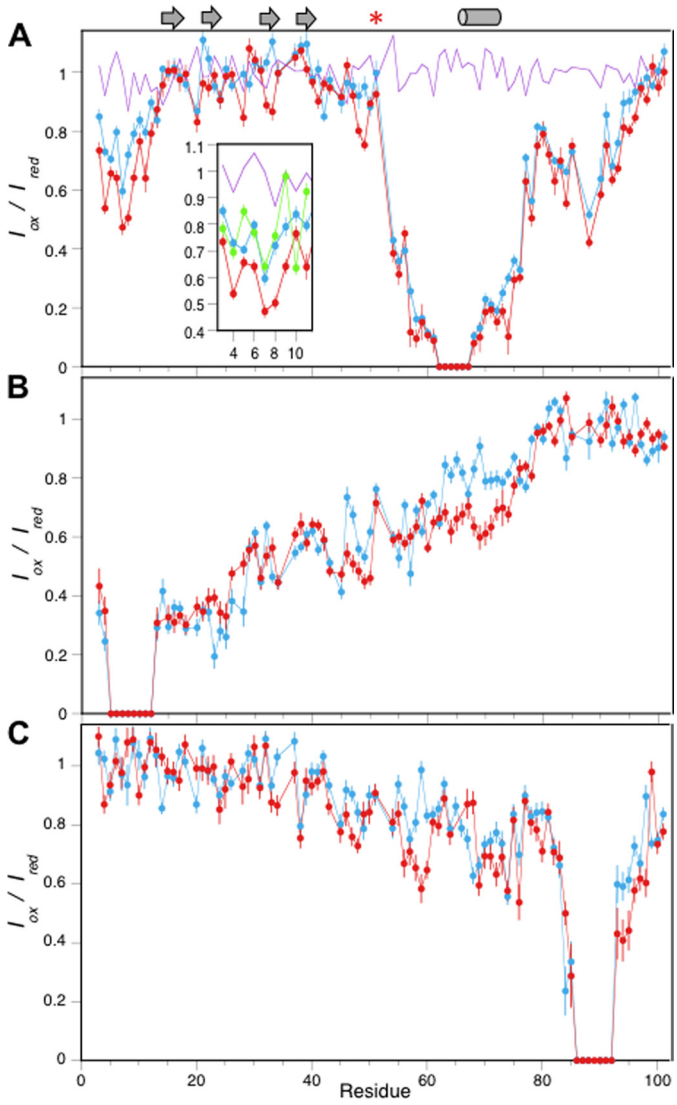

FIGURE 7. **Long-range interactions in PAGE4 from PRE measurements.** *A*, Cys-63-MTSL PRE data for backbone amide protons of non-phosphorylated PAGE4 (*blue*) and Thr(P)-51 PAGE4 (*red*). Results from a control experiment (*purple*) indicate that the observed effects are intramolecular (see "Experimental Procedures" for details). *Inset*, the effect of phosphorylation at Ser-9 (*green*) on the PRE data for the N-terminal basic motif. The conformational preferences of the polypeptide chain (*gray symbols*) and the primary phosphorylation site (*red asterisk*) are indicated. *B*, S7C-MTSL PRE data for non-phosphorylated PAGE4 (*blue*) and Thr(P)-51 PAGE4 (*red*). *C*, N88C-MTSL PRE data for non-phosphorylated PAGE4 (*blue*) and Thr(P)-51 PAGE4 (*red*). Errors in I_{ox}/I_{red} values are estimated from the uncertainty in peak intensity measurements.

vide a useful framework for visualizing preferred states of the highly flexible ensemble. For clarity, separate calculations were performed for long-range interactions between the central acidic region and the N- and C-terminal contact sites. Therefore, WT PAGE4, on average, populates conformations where the highly basic N-terminal motif (RVRSRSRGR) is within 25 Å of the central acidic region (Glu-43, Glu-47, Glu-49, Glu-55, Glu-56, Glu-60, and Asp-62) neighboring Cys-63 (Fig. 8*A*). Phosphorylation at Thr-51 increases the negative charge in this acidic region and induces turn-like structures that provide a more compact transient interaction with the N-terminal motif (Fig. 8*B*). Secondary phosphorylation at Ser-9 lowers the net positive charge of the N-terminal basic motif, with weakening of the PRE effect (Fig. 7*A*, *inset*). The interaction between these two regions, therefore, appears to be driven mostly by favorable electrostatic effects. In addition, other interactions between a C-terminal motif centered on residue Asn-88 and the transient helix contribute to the overall conformational ensemble. These long-range contacts may also be at least partly due to electrostatic interactions of several basic residues in this region (Lys-82, Lys-84, Lys-90, Lys-93, and Lys-K95) with central acidic amino acids (Fig. 8, *C* and *D*). Notably, both the N- and C-terminal contacts to the central acidic region decrease accessibility to the transient helix.

Backbone Flexibility and the Effect of Phosphorylation—Steady-state ^{1}H-^{15}N heteronuclear NOE measurements, which report on picosecond-nanosecond timescale motions in the backbone, were made for both WT PAGE4 and phospho-PAGE4 (Fig. 9). These data show that WT PAGE4 is highly flexible, with average heteronuclear NOE values (~0.1–0.2) similar to those of comparable molecular weight IDPs (53). However, flexibility is not uniform across the polypeptide chain. Residues 67–73 have elevated ^{1}H-^{15}N NOE values (~0.3–0.4), indicating increased rigidity for the transiently ordered helical region relative to other parts of the sequence. In contrast, residues 30–33 comprise a flexible internal region with negative heteronuclear NOE values comparable with those of amino acids near the termini. Phosphorylation on Thr-51 decreases picosecond-nanosecond timescale motions in the immediate vicinity, with higher heteronuclear NOE values for Thr-51, Ile-54, and Glu-55 and smaller changes in other parts of the chain. Similar effects were seen at higher temperatures (data not shown).

Functional Studies—NMR-based ligand binding experiments were used to define the PAGE4 binding interface with human c-Jun. A series of unlabeled c-Jun fragments, 1–61, 1–90, 1–150, 1–223, and full-length c-Jun, were tested individually with ^{15}N-labeled WT PAGE4 and phospho-PAGE4. Chemical shift perturbation experiments with the shorter c-Jun fragments, 1–61, 1–90, and 1–150, showed no change in two-dimensional ^{15}N HSQC spectra of WT PAGE4 with up to 6 equivalents of c-Jun fragment added. In contrast, addition of either unlabeled full-length c-Jun or c-Jun (1–223) perturbed a specific set of WT PAGE4 residues in a similar way, albeit weakly (Fig. 10*A*). The largest chemical shift changes occurred in the transient helix region of PAGE4 from residues 69–73 (Fig. 10, *A* and *C*). The binding interaction between WT PAGE4 and c-Jun was estimated at a K_D of >50 μM from the NMR titration data, with precipitation of c-Jun at higher concentrations preventing a more accurate determination. Phosphorylation of PAGE4 on Thr-51 significantly attenuates binding at the helical interface with c-Jun at residues 69–73 (Fig. 10, *B* and *C*). These NMR-based observations agree well with earlier single-molecule FRET studies (14, 18), which showed that the c-Jun binding site is in the C-terminal half of PAGE4 and that affinity for c-Jun decreases upon phosphorylation of Thr-51. Therefore, the NMR results presented here provide a higher-resolution identification of the transient helical region of PAGE4 as the binding site with c-Jun. In addition, reverse titration experiments using a ^{15}N-labeled c-Jun fragment (residues 150–331) and unlabeled WT PAGE4 exhibited chemical shift perturba-

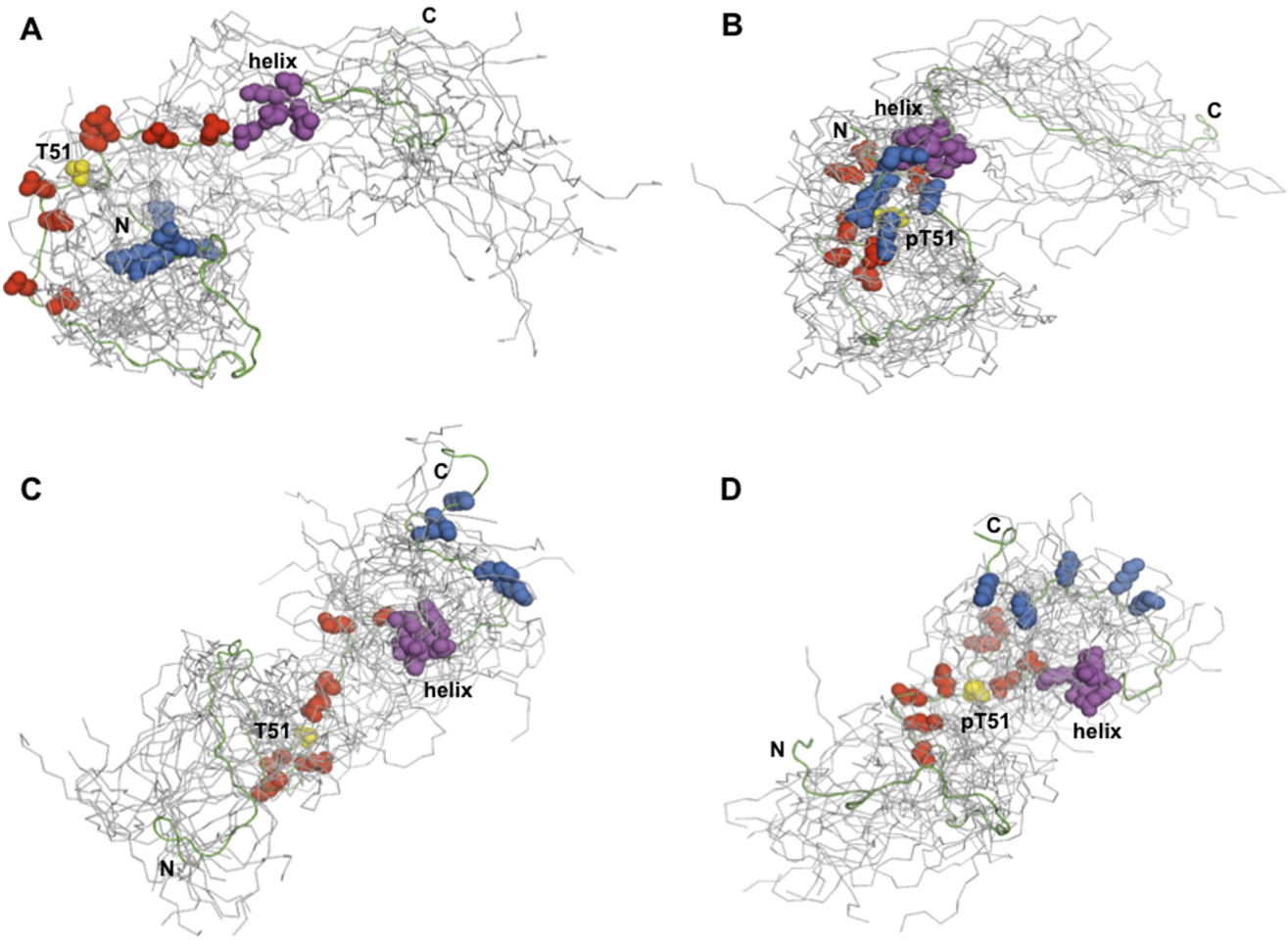

FIGURE 8. **Model for phosphorylation-induced conformational ensemble switching in PAGE4.** *A*, the non-phosphorylated PAGE4 adopts preferred transient structures such as the one highlighted from an ensemble of the 20 lowest energy conformers, where, on average, the N-terminal basic motif (*blue spheres*; Arg-4, Arg-6, Arg-8, Arg-10, and Arg-12) interacts weakly with the central acidic region (*red spheres*; Glu-43, Glu-47, Glu-49, Glu-55, Glu-56, Glu-60, and Asp-62) neighboring Thr-51 (*yellow*). *B*, upon phosphorylation at Thr-51, the central region becomes more compact and more negatively charged, decreasing the average distance between Thr(P)-51, the basic motif, and the transient helix (*magenta*). *C* and *D*, models of the transient interaction between the central acidic region and the C-terminal basic motif (*blue spheres*; Lys-82, Lys-84, Lys-90, Lys-93, and Lys-95) in non-phosphorylated PAGE4 (*C*) and Thr(P)-51 PAGE4 (*D*). The total number of distance restraints used was as follows: *A*, 51; *B*, 55; *C*, 53; *D*, 61.

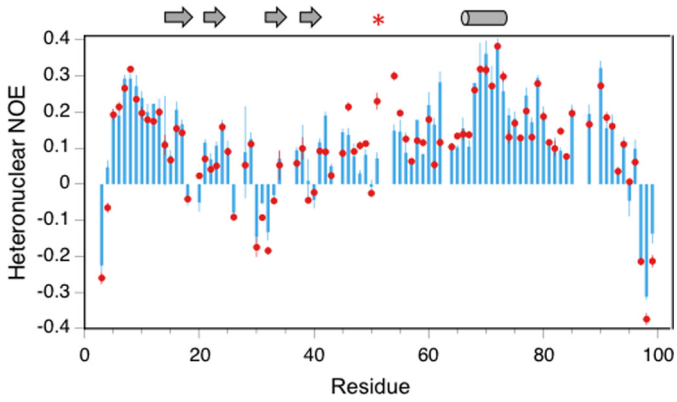

FIGURE 9. **Backbone dynamics in PAGE4.** Plot of the ^{1}H-^{15}N steady-state heteronuclear NOE *versus* residue number for WT PAGE4 (*blue*) and Thr(P)-51 PAGE4 (*red*). Higher values indicate decreased flexibility of the polypeptide chain. *Error bars* indicate mean ± S.D.

tions and peak intensity decreases consistent with a weak binding interaction (Fig. 10*D*).

Because the c-Jun (1–223) fragment, but not shorter constructs, gave similar NMR results as full-length c-Jun, residues 150–223 must be important for the interaction with PAGE4. This region is adjacent to the basic DNA-binding domain of c-Jun, which extends from residues 257–276. Consistent with the NMR binding data, results from a luciferase assay in a PC3 prostate cancer cell line with truncated c-Jun fragments demonstrated that PAGE4-mediated amplification of c-Jun transactivation was negligible and required inclusion of the region from 150–223 (Fig. 10*E*). An additional mutant of PAGE4, lacking most of the N-terminal basic motif from residues 5–11, had a small (~3-fold) but significant increase in c-Jun transactivation (Fig. 10*F*). The N-terminal motif therefore appears to have a partial autoinhibitory effect on the cellular function of PAGE4, possibly through its long-range interactions with the central region.

Discussion

Comparison with Other PAGE Family Members—The only other cancer/testis antigen studied in detail using biophysical methods is PAGE5 (29). However, the role of posttranslational modifications in PAGE5 remains unknown. PAGE4 has 43% sequence identity to PAGE5 (Fig. 1*A*), and, although there is

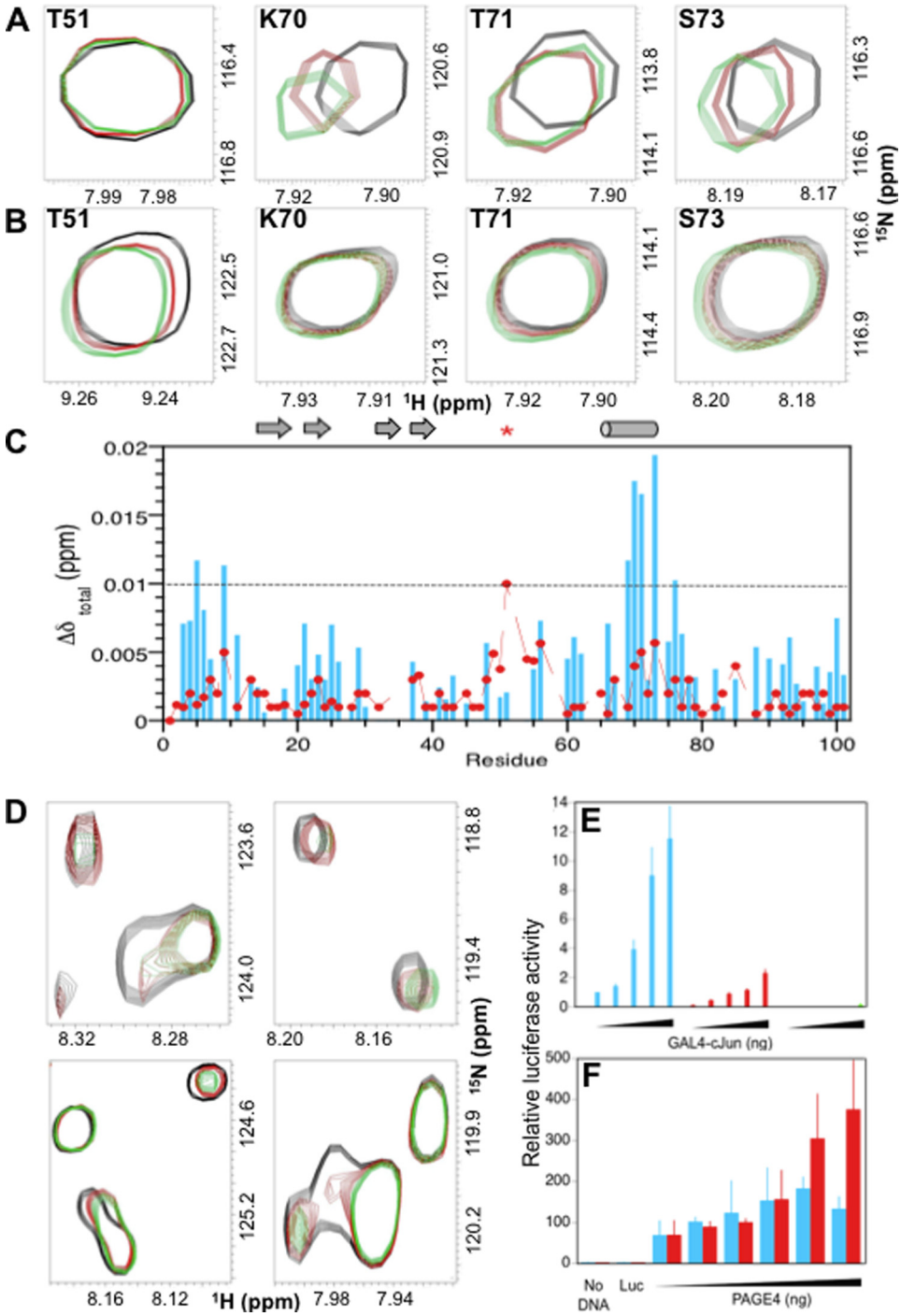

FIGURE 10. **Summary of functional studies.** *A*, regions from two-dimensional ^{1}H-^{15}N HSQC spectra in the titration of ^{15}N-labeled WT PAGE4 with unlabeled c-Jun showing superimposed control (*black*), 1:1.5 PAGE4/c-Jun (*red*), and 1:3 PAGE4/c-Jun (*green*) spectra. *B*, similar regions using ^{15}N-labeled Thr(P)-51 PAGE4 with unlabeled c-Jun at the same molar ratios as for *A*. *C*, chemical shift perturbation plot for WT PAGE4 (*blue*) and Thr(P)-51 PAGE4 (*red*) as a function of residue number. Values of $\Delta\delta_{total}$ below the *dashed line* are estimated to be within the experimental error for measuring chemical shift changes. *D*, regions from two-dimensional ^{1}H-^{15}N HSQC spectra in the titration of ^{15}N-labeled c-Jun (residues 150–331) with unlabeled WT PAGE4 showing superimposed control (*black*), 1:2 c-Jun/PAGE4 (*red*), and 1:4 c-Jun/PAGE4 (*green*) spectra. *E*, cell-based luciferase assay measuring the ability of WT PAGE4 to potentiate c-Jun transactivation using different lengths of c-Jun constructs: *blue*, c-Jun (1–223); *red*, c-Jun (1–150); *green*, c-Jun (1–61). The GAL4-c-Jun DNA amounts were 6.25, 12.5, 25, 50, and 100 ng. *F*, luciferase assay monitoring c-Jun transactivation levels in the presence of either WT PAGE4 (*blue*) or the ΔN (5–11) mutant (*red*). The PAGE4 DNA amounts were 0, 10, 20, 30, 75, and 150 ng. *Error bars* are mean ± S.D. in *D* and *E*.

some overlap in the structural tendencies of these two proteins, there are also numerous differences at the per-residue level. PAGE4 has more β-type extended structure propensity than PAGE5, localized in the N-terminal half for both proteins but in different positions. The single β structure in PAGE5 is in a region that is largely deleted in PAGE4. Residues that are central to this β-extended structure in PAGE5 correspond with a highly flexible internal region (residues 30–32) in PAGE4. Notably, seven of the 11 prolines in PAGE4 have a PX_7-PX_7-PPX_7-PX_7PP sequence motif from residues 19–53 that does not

occur in the other PAGE family members and likely contributes to these conformational tendencies. A similar sequence motif with disordered extended conformations has been observed in a pollen allergen (54). There are also differences in the helical preferences of PAGE4 and PAGE5. The transient helix in PAGE4 (residues 65–73) is nine residues long, whereas the helix in PAGE5 consists of 16 amino acids and starts nine residues earlier, corresponding with a region in PAGE4 that increases its turn-like structure upon phosphorylation at Thr-51. Significantly, a phosphorylation site corresponding to Thr-51 is not present in PAGE5 or any of the other PAGE sequences. Indeed, the region that is phosphorylated and populates turn-like structures in PAGE4 is the most variable stretch of amino acid sequence across the entire PAGE family. Furthermore, the highly basic R*X*R*X*R*X*R*X*R motif at the N terminus of PAGE4 that interacts transiently with the central acidic region is not present in PAGE5. Together, these observations suggest different conformational modes of action for the PAGE proteins.

Effect of Phosphorylation on PAGE4 Conformation and Dynamics—Site-specific phosphorylation at Thr-51 alters the conformational preferences of PAGE4, increasing the population of turn-like structures and the rigidity of the backbone in the central region. In addition, there are long-range transient interactions between basic motifs and the central acidic region (Fig. 8) that impose further constraints on the distribution of populations in the ensemble while maintaining overall chain flexibility. Previous single-molecule FRET studies on PAGE4 also indicated a restriction of the polypeptide chain upon phosphorylation (18). Therefore, phosphorylation switches the conformational ensemble to a more compact but still flexible state.

The increase in turn-like structures upon phosphorylation has been observed previously in NMR studies of other intrinsically disordered proteins, such as amyloid precursor protein (55) and the serine/arginine-rich protein SRSF1 (56). This may be due to increased electrostatic interactions of the phosphoryl group with nearby basic residues. In the case of PAGE4, interactions of Thr(P)-51 with Arg-48 and Arg-57 would increase turn populations, for example. Additionally, phosphorylation provides new H-bond acceptors for main chain N-H groups to interact with transiently. Unlike PAGE4, long-range effects do not appear to be detected in amyloid precursor protein and SRSF1. In one recent example, however, phosphorylation of an IDP, 4E-BP2, provides sufficient long-range interactions to weakly stabilize a folded domain (57). This demonstrates that some IDPs are only marginally unstable. Posttranslational modifications can induce shifts in the ensemble that may increase H-bonding or other energetically favorable interactions. Therefore, phosphorylation of IDPs appears to lead to a continuum of structure-promoting effects where PAGE4 is between amyloid precursor protein and 4E-BP2. Moreover, the structural ensemble shifts induced by posttranslational modifications seen here and elsewhere (57–59) are comparable with the conformational switching events in some marginally stable folded proteins in response to mutation or environmental triggers (60, 61).

Effect of Phosphorylation on Function—Phosphorylation of PAGE4 at Thr-51 has significant effects on its function. At the cellular level, Thr(P)-51 PAGE4 potentiates c-Jun transactivation ~30-fold over non-phosphorylated PAGE4 (18). Interestingly, at the biochemical level, phosphorylation of PAGE4 attenuates binding to c-Jun (Fig. 10, *B* and *C*), similar to results for other IDPs where phosphorylation causes loss of a binding function (62, 63). In such cases, the decreased affinity may be due to phosphorylation-induced destabilization of a binding competent state such as a helix (64) or because of other effects such as masking interactions (65, 66). For PAGE4, phosphorylation does not appear to destabilize the helical region but actually leads to a slightly increased helical character (Fig. 5*A*). Therefore, one plausible reason for the lowered affinity of Thr(P)-51 PAGE4 for c-Jun *in vitro* may be the more compact nature of the ensemble in the phosphorylated state compared with unphosphorylated PAGE4 (Fig. 8). The NMR-based structural models indicate that the elevated level of medium- and long-range contacts in Thr(P)-51 PAGE4 decreases accessibility to the helical region. Because this is the region shown to bind to c-Jun, the attenuation in binding due to phosphorylation may be due occlusion effects (Fig. 8, *B* and *D*). Indeed, the transient long-range interaction involving the N-terminal basic motif appears to play a role in cellular function. This is evident from the observation that deletion of residues 5–11 leads to a modest but significant increase in c-Jun transactivation, suggesting a weak autoinhibitory effect. Similar effects have been reported in other IDPs (59, 66, 67).

Additional factors may be involved in the PAGE4/c-Jun interaction that could contribute to higher affinity and further ordering of PAGE4. To account for its strongly amplifying effect on c-Jun transactivation, it has been suggested that Thr(P)-51 PAGE4 has increased affinity for another, as yet undetermined factor (18). Possible candidates for this factor are proteins in the Fos family, c-Fos, FRA1, and FRA2, which are known to heterodimerize with c-Jun to form AP-1 complexes (68) and have up-regulated RNA patterns coincident with PAGE4, as discerned by querying NCBI GEO. Finally, a PSI-BLAST analysis of the PAGE4 sequence against the Protein Data Bank showed that it has a 47-amino acid region (residues 53–99) with significant sequence similarity (30% identity, 49% similarity) to the disordered tether of human SAP-1. SAP-1 stabilizes a homodimeric transcription factor-DNA complex that plays a role in regulating c-*fos* expression (69). We hypothesize that PAGE4 carries out its positive regulator role by stabilizing a Jun-Fos-type complex in a similar way. Further experiments will be required on the AP-1 complex to test this hypothesis and determine the full extent of the role of PAGE4 in c-Jun transactivation.

Author Contributions—Y. H., Y. C., E. S., and K. W. expressed recombinant proteins and performed NMR experiments. S. M. M., K. R., and A. B. carried out transactivation assays. P. N. B. provided expression constructs and purification protocols. P. K. and J. O. wrote the manuscript.

Acknowledgments—We thank Lauren Porter and Nese Sari for discussions. We also thank Alex Grishaev for assistance with implementing radius of gyration restraints in ensemble calculations.

References

1. Scanlan, M. J., Gure, A. O., Jungbluth, A. A., Old, L. J., and Chen, Y. T. (2002) Cancer/testis antigens: an expanding family of targets for cancer immunotherapy. *Immunol. Rev.* **188,** 22–32
2. Simpson, A. J., Caballero, O. L., Jungbluth, A., Chen, Y. T., and Old, L. J. (2005) Cancer/testis antigens, gametogenesis and cancer. *Nat. Rev. Cancer* **5,** 615–625
3. Almeida, L. G., Sakabe, N. J., deOliveira, A. R., Silva, M. C., Mundstein, A. S., Cohen, T., Chen, Y. T., Chua, R., Gurung, S., Gnjatic, S., Jungbluth, A. A., Caballero, O. L., Bairoch, A., Kiesler, E., White, S. L., Simpson, A. J., Old, L. J., Camargo, A. A., and Vasconcelos, A. T. (2009) CTdatabase: a knowledge-base of high-throughput and curated data on cancer-testis antigens. *Nucleic Acids Res.* **37,** 816–819
4. Stevenson, B. J., Iseli, C., Panji, S., Zahn-Zabal, M., Hide, W., Old, L. J., Simpson, A. J., and Jongeneel, C. V. (2007) Rapid evolution of cancer/testis genes on the X chromosome. *BMC Genomics* **8,** 129–229
5. Dobrynin, P., Matyunina, E., Malov, S. V., and Kozlov, A. P. (2013) The novelty of human cancer/testis antigen encoding genes in evolution. *Int. J. Genomics* 10.1155/2013/105108
6. Kalejs, M., and Erenpreisa, J. (2005) Cancer/testis antigens and gametogenesis: a review and "brain-storming" session. *Cancer Cell Int.* **5,** 4–14
7. Whitehurst, A. W. (2014) Cause and consequence of cancer/testis antigen activation in cancer. *Annu. Rev. Pharmacol. Toxicol.* **54,** 251–272
8. Rajagopalan, K., Mooney, S. M., Parekh, N., Getzenberg, R. H., and Kulkarni, P. (2011) A majority of the cancer/testis antigens are intrinsically disordered proteins. *J. Cell Biochem.* **112,** 3256–3267
9. Yoon, M. K., Mitrea, D. M., Ou, L., and Kriwacki, R. W. (2012) Cell cycle regulation by the intrinsically disordered proteins p21 and p27. *Biochem. Soc. Trans.* **40,** 981–988
10. Uversky, V. N. (2013) Unusual biophysics of intrinsically disordered proteins. *Biochim. Biophys. Acta* **1834,** 932–951
11. Wright, P. E., and Dyson, H. J. (2015) Intrinsically disordered proteins in cellular signaling and regulation. *Nat. Rev. Mol. Cell Biol.* **16,** 18–29
12. Zeng, Y., Wodzenski, D., Gao, D., Shiraishi, T., Terada, N., Li, Y., Vander Griend, D. J., Luo, J., Kong, C., Getzenberg, R. H., and Kulkarni, P. (2013) Prostate-associated gene 4 (PAGE4) protects cells against stress by elevating p21 and suppressing reactive oxygen species production. *Am. J. Clin. Exptl. Urol.* **1,** 39–52
13. Prakash, K., Pirozzi, G., Elashoff, M., Munger, W., Waga, I., Dhir, R., Kakehi, Y., and Getzenberg, R. H. (2002) Symptomatic and asymptomatic benign prostatic hyperplasia: molecular differentiation by using microarrays. *Proc. Natl. Acad. Sci. U.S.A.* **99,** 7598–7603
14. Rajagopalan, K., Qiu, R., Mooney, S. M., Rao, S., Shiraishi, T., Sacho, E., Huang, H., Shapiro, E., Weninger, K. R., Kulkarni, P. (2014) The stress-response protein prostate-associated gene 4, interacts with c-Jun and potentiates its transactivation. *Biochim. Biophys. Acta* **1842,** 154–163
15. Bull, J. H., Ellison, G., Patel, A., Muir, G., Walker, M., Underwood, M., Khan, F., and Paskins, L. (2001) Identification of potential diagnostic markers of prostate cancer and prostatic intraepithelial neoplasia using cDNA microarray. *Br. J. Cancer* **84,** 1512–1519
16. Sampson, N., Ruiz, C., Zenzmaier, C., Bubendorf, L., and Berger, P. (2012) PAGE4 positivity is associated with attenuated AR signaling and predicts patient survival in hormone-naïve prostate cancer. *Am. J. Pathol.* **181,** 1443–1454
17. Zeng, Y., He, Y., Yang, F., Mooney, S. M., Getzenberg, R. H., Orban, J., and Kulkarni, P. (2011) The cancer/testis antigen prostate-associated gene 4 (PAGE4) is a highly intrinsically disordered protein. *J. Biol. Chem.* **286,** 13985–13994
18. Mooney, S. M., Qiu, R., Kim, J. J., Sacho, E. J., Rajagopalan, K., Johng, D., Shiraishi, T., Kulkarni, P., and Weninger, K. R. (2014) Cancer/testis antigen PAGE4, a regulator of c-Jun transactivation, is phosphorylated by homeodomain-interacting protein kinase 1, a component of the stress-response pathway. *Biochemistry* **53,** 1670–1679
19. Leppä, S., and Bohmann, D. (1999) Diverse functions of JNK signaling and c-Jun in stress response and apoptosis. *Oncogene* **18,** 6158–6162
20. Li, W., Wu, C. L., Febbo, P. G., and Olumi, A. F. (2007) Stromally expressed c-Jun regulates proliferation of prostate epithelial cells. *Am. J. Pathol.* **171,** 1189–1198
21. Sato, N., Sadar, M. D., Bruchovsky, N., Saatcioglu, F., Rennie, P. S., Sato, S., Lange, P. H., and Gleave, M. E. (1997) Androgenic induction of prostate-specific antigen gene is repressed by protein-protein interaction between the androgen receptor and AP-1/c-Jun in the human prostate cancer cell line LNCaP. *J. Biol. Chem.* **272,** 17485–17494
22. Edwards, J., Krishna, N. S., Mukherjee, R., and Bartlett, J. M. (2004) The role of c-Jun and c-Fos expression in androgen-independent prostate cancer. *J. Pathol.* **204,** 153–158
23. Chen, S. Y., Cai, C., Fisher, C. J., Zheng, Z., Omwancha, J., Hsieh, C. L., and Shemshedini, L. (2006) c-Jun enhancement of androgen receptor transactivation is associated with prostate cancer cell proliferation. *Oncogene* **25,** 7212–7223
24. Cai, C., Hsieh, C. L., and Shemshedini, L. (2007) c-Jun has multiple enhancing activities in the novel cross talk between the androgen receptor and Ets variant gene 1 in prostate cancer. *Mol. Cancer Res.* **5,** 725–735
25. Kajanne, R., Miettinen, P., Tenhunen, M., and Leppä, S. (2009) Transcription factor AP-1 promotes growth and radioresistance in prostate cancer cells. *Int. J. Oncol.* **35,** 1175–1182
26. Sun, T., Yang, M., Chen, S., Balk, S., Pomerantz, M., Hsieh, C. L., Brown, M., Lee, G. S., and Kantoff, P. W. (2012) The altered expression of MiR-221/-222 and MiR-23b/-27b is associated with the development of human castration resistant prostate cancer. *Prostate* **72,** 1093–1103
27. Lin-Tsai, O., Clark, P. E., Miller, N. L., Fowke, J. H., Hameed, O., Hayward, S. W., and Strand, D. W. (2014) Surgical intervention for symptomatic benign prostatic hyperplasia is correlated with expression of the AP-1 transcription factor network. *Prostate* **74,** 669–679
28. Ouyang, X., Jessen, W. J., Al-Ahmadie, H., Serio, A. M., Lin, Y., Shih, W. J., Reuter, V. E., Scardino, P. T., Shen, M. M., Aronow, B. J., Vickers, A. J., Gerald, W. L., and Abate-Shen, C. (2008) Activator protein-1 transcription factors are associated with progression and recurrence of prostate cancer. *Cancer Res.* **68,** 2132–2144
29. Hellman, M., Tossavainen, H., Rappu, P., Heino, J., and Permi, P. (2011) Characterization of intrinsically disordered prostate associated gene (PAGE5) at single residue resolution by NMR spectroscopy. *PLoS ONE* **6,** e26633
30. Murzin, A. G. (2008) Biochemistry: metamorphic proteins. *Science* **320,** 1725–1726
31. Bryan, P. N., and Orban, J. (2010) Proteins that switch folds. *Curr. Opin. Struct. Biol.* **20,** 482–488
32. Ruan, B., Fisher, K. E., Alexander, P. A., Doroshko, V., and Bryan, P. N. (2004) Engineering subtilisin into a fluoride-triggered processing protease useful for one-step protein purification. *Biochemistry* **43,** 14539–14546
33. Bradford, M. M. (1976) Rapid and sensitive method for the quantitation of microgram quantities of protein utilizing the principle of protein-dye binding. *Anal. Biochem.* **72,** 248–254
34. Delaglio, F., Grzesiek, S., Vuister, G. W., Zhu, G., Pfeifer, J., and Bax, A. (1995) NMRPipe: a multidimensional spectral processing system based on UNIX pipes. *J. Biomol. NMR* **6,** 277–293
35. Goddard, T. D., and Kneller, D. G. (2004) *SPARKY 3*, University of California, San Francisco
36. Kjaergaard, M., and Poulsen, F. M. (2011) Sequence correction of random coil chemical shifts: correlation between neighbor correction factors and changes in the Ramachandran distribution. *J. Biomol. NMR* **50,** 157–165
37. Vuister, G. W., and Bax, A. (1993) Quantitative J correlation: A new approach for measuring homonuclear three-bond $J(H^N H^\alpha)$ coupling constants in ^{15}N-enriched proteins. *J. Am. Chem. Soc.* **115,** 7772–7777
38. Plaxco, K. W., Morton, C. J., Grimshaw, S. B., Jones, J. A., Pitkeathly, M., Campbell, I. D., and Dobson, C. M. (1997) The effects of guanidine hydrochloride on the "random coil" conformations and NMR chemical shifts of the peptide series GGXGG. *J. Biomol. NMR* **10,** 221–230
39. Farrow, N. A., Muhandiram, R., Singer, A. U., Pascal, S. M., Kay, C. M., Gish, G., Shoelson, S. E., Pawson, T., Forman-Kay, J. D., and Kay, L. E. (1994) Backbone dynamics of a free and phosphopeptide-complexed Src homology 2 domain studied by ^{15}N NMR relaxation. *Biochemistry* **33,** 5984–6003
40. Hwang, T. L., van Zijl, P. C., and Mori, S. (1998) Accurate quantitation of water-amide proton exchange rates using the phase-modulated CLEAN

chemical exchange (CLEANEX-PM) approach with a fast-HSQC (FHSQC) detection scheme. *J. Biomol. NMR* **11,** 221–226
41. Brünger, A. T., Adams, P. D., Clore, G. M., DeLano, W. L., Gros, P., Grosse-Kunstleve, R. W., Jiang, J. S., Kuszewski, J., Nilges, M., Pannu, N. S., Read, R. J., Rice, L. M., Simonson, T., and Warren, G. L. (1998) Crystallography and NMR system: a new software suite for macromolecular structure determination. *Acta Crystallogr. D Biol. Crystallogr.* **54,** 905–921
42. Kuszewski, J., Gronenborn, A. M., and Clore, G. M. (1999) Improving the packing and accuracy of NMR structures with a pseudopotential for the radius of gyration. *J. Am. Chem. Soc.* **121,** 2337–2338
43. DeLano, W. L. (2012) The PyMOL Molecular Graphics System, version 1.5.0.1, Schroedinger, LLC, New York
44. Panchal, S. C., Bhavesh, N. S., and Hosur, R. V. (2001) Improved 3D triple resonance experiments, HNN and HN(C)N, for H^N and ^{15}N sequential correlations in (^{13}C, ^{15}N) labeled proteins: application to unfolded proteins. *J. Biomol. NMR* **20,** 135–147
45. Mukrasch, M. D., Bibow, S., Korukottu, J., Jeganathan, S., Biernat, J., Griesinger, C., Mandelkow, E., and Zweckstetter, M. (2009) Structural polymorphism of 441-residue Tau at single residue resolution. *PLoS Biol.* **7,** e1000034
46. Wishart, D. S., and Sykes, B. D. (1994) The ^{13}C chemical-shift index: a simple method for the identification of protein secondary structure using ^{13}C chemical-shift data. *J. Biomol. NMR* **4,** 171–180
47. Saitô, H., Ando, I., and Ramamoorthy, A. (2010) Chemical shift tensor: the heart of NMR: insights into biological aspects of proteins. *Prog. Nucl. Magn. Reson. Spectrosc.* **57,** 181–228
48. Kjaergaard, M., Brander, S., and Poulsen, F. M. (2011) Random coil chemical shift for intrinsically disordered proteins: effects of temperature and pH. *J. Biomol. NMR* **49,** 139–149
49. Shen, Y., and Bax, A. (2010) Prediction of Xaa-Pro peptide bond conformation from sequence and chemical shifts. *J. Biomol. NMR* **46,** 199–204
50. Englander, S. W., and Kallenbach, N. R. (1983) Hydrogen exchange and structural dynamics of proteins and nucleic acids. *Q. Rev. Biophys.* **16,** 521–655
51. Orban, J., Alexander, P., Bryan, P., and Khare, D. (1995) Assessment of stability differences in the protein G B1 and B2 domains from hydrogen-deuterium exchange: comparison with calorimetric data. *Biochemistry* **34,** 15291–15300
52. Gillespie, J. R., and Shortle, D. (1997) Characterization of long-range structure in the denatured state of staphylococcal nuclease: I: paramagnetic relaxation enhancement by nitroxide spin labels. *J. Mol. Biol.* **268,** 158–169
53. Sung, Y.-H., and Eliezer, D. (2007) Residual structure, backbone dynamics, and interactions within the synuclein family. *J. Mol. Biol.* **372,** 689–707
54. Razzera, G., Gadermaier, G., de Paula, V., Almeida, M. S., Egger, M., Jahn-Schmid, B., Almeida, F. C., Ferreira, F., and Valente, A. P. (2010) Mapping the interactions between a major pollen allergen and human IgE antibodies. *Structure* **18,** 1011–1021
55. Ramelot, T. A., and Nicholson, L. K. (2001) Phosphorylation-induced structural changes in the amyloid precursor protein cytoplasmic tail detected by NMR. *J. Mol. Biol.* **307,** 871–884
56. Xiang, S., Gapsys, V., Kim, H.-Y., Bessonov, S., Hsiao, H.-H., Möhlmann, S., Klaukien, V., Ficner, R., Becker, S., Urlaub, H., Lührmann, R., de Groot, B., and Zweckstetter, M. (2013) Phosphorylation drives a dynamic switch in serine/arginine-rich proteins. *Structure* **21,** 2162–2174
57. Bah, A., Vernon, R. M., Siddiqui, Z., Krzeminski, M., Muhandiram, R., Zhao, C., Sonenberg, N., Kay, L. E., and Forman-Kay, J. D. (2015) Folding of an intrinsically disordered protein by phosphorylation as a regulatory switch. *Nature* **519,** 106–109
58. Cordek, D. G., Croom-Perez, T. J., Hwang, J., Hargittai, M. R., Subba-Reddy, C. V., Han, Q., Lodeiro, M. F., Ning, G., McCrory, T. S., Arnold, J. J., Koc, H., Lindenbach, B. D., Showalter, S. A., Cameron, C. E. (2014) Expanding the proteome of an RNA virus by phosphorylation of an intrinsically disordered viral protein. *J. Biol. Chem.* **289,** 24397–24416
59. Stott, K., Watson, M., Bostock, M. J., Mortensen, S. A., Travers, A., Grasser, K. D., Thomas, J. O. (2014) Structural insights into the mechanism of negative regulation of single-box high mobility group proteins by the acidic tail domain. *J. Biol. Chem.* **289,** 29817–29826
60. Tuinstra, R. L., Peterson, F. C., Kutlesa, S., Elgin, E. S., Kron, M. A., and Volkman, B. F. (2008) Interconversion between two unrelated protein folds in the lymphotactin native state. *Proc. Natl. Acad. Sci. U.S.A.* **105,** 5057–5062
61. He, Y., Chen, Y., Alexander, P. A., Bryan, P. N., and Orban, J. (2012) Mutational tipping points for switching protein folds and functions. *Structure* **20,** 283–291
62. Sakaguchi, K., Saito, S., Higashimoto, Y., Roy, S., Anderson, C. W., and Appella, E. (2000) Damage-mediated phosphorylation of human p53 threonine 18 through a cascade mediated by a casein 1-like kinase: effect on Mdm2 binding. *J. Biol. Chem.* **275,** 9278–9283
63. Huang, K. L., Chadee, A. B., Chen, C. Y., Zhang, Y., and Shyu, A. B. (2013) Phosphorylation at intrinsically disordered regions of PAM2 motif-containing proteins modulates their interactions with PABPC1 and influences mRNA fate. *RNA* **19,** 295–305
64. Jabbur, J. R., Tabor, A. D., Cheng, X., Wang, H., Uesugi, M., Lozano, G., and Zhang, W. (2002) Mdm-2 binding and TAF(II)31 recruitment is regulated by hydrogen bond disruption between the p53 residues Thr18 and Asp21. *Oncogene* **21,** 7100–7113
65. Andresen, C., Helander, S., Lemak, A., Farès, C., Csizmok, V., Carlsson, J., Penn, L. Z., Forman-Kay, J. D., Arrowsmith, C. H., Lundström, P., and Sunnerhagen, M. (2012) Transient structure and dynamics in the disordered c-Myc transactivation domain affect Bin1 binding. *Nucleic Acids Res.* **40,** 6353–6366
66. Bista, M., Petrovich, M., and Fersht, A. R. (2013) MDMX contains an autoinhibitory sequence element. *Proc. Natl. Acad. Sci. U.S.A.* **110,** 17814–17819
67. Trudeau, T., Nassar, R., Cumberworth, A., Wong, E. T., Woollard, G., and Gsponer, J. (2013) Structure and intrinsic disorder in protein autoinhibition. *Structure* **21,** 332–341
68. Glover, J. N., and Harrison, S. C. (1995) Crystal structure of the heterodimeric bZIP transcription factor c-Fos-c-Jun bound to DNA. *Nature* **373,** 257–261
69. Hassler, M., and Richmond, T. J. (2001) The B-box dominates SAP-1-SRF interactions in the structure of the ternary complex. *EMBO J.* **20,** 3018–3028